

Aspect ratio dependence of heat transport by turbulent Rayleigh-Bénard convection in rectangular cells

Quan ZHOU[†], Bo-Fang LIU, Chun-Mei LI and Bao-Chang ZHONG

Shanghai Institute of Applied Mathematics and Mechanics, and Shanghai Key Laboratory of Mechanics in Energy Engineering, Shanghai University, Shanghai 200072, China

(Received ?? and in revised form ??)

We report high-precision measurements of the Nusselt number Nu as a function of the Rayleigh number Ra in water-filled rectangular Rayleigh-Bénard convection cells. The horizontal length L and width W of the cells are 50.0 cm and 15.0 cm, respectively, and the heights $H = 49.9, 25.0, 12.5, 6.9, 3.5,$ and 2.4 cm, corresponding to the aspect ratios $(\Gamma_x \equiv L/H, \Gamma_y \equiv W/H) = (1, 0.3), (2, 0.6), (4, 1.2), (7.3, 2.2), (14.3, 4.3),$ and $(20.8, 6.3)$. The measurements were carried out over the Rayleigh number range $6 \times 10^5 \lesssim Ra \lesssim 10^{11}$ and the Prandtl number range $5.2 \lesssim Pr \lesssim 7$. Our results show that for rectangular geometry turbulent heat transport is independent of the cells' aspect ratios and hence is insensitive to the nature and structures of the large-scale mean flows of the system. This is slightly different from the observations in cylindrical cells where Nu is found to be in general a decreasing function of Γ , at least for $\Gamma = 1$ and larger. Such a difference is probably a manifestation of the finite plate conductivity effect. Corrections for the influence of the finite conductivity of the top and bottom plates are made to obtain the estimates of Nu_∞ for plates with perfect conductivity. The local scaling exponents β_l of $Nu_\infty \sim Ra^{\beta_l}$ are calculated and found to increase from 0.243 at $Ra \simeq 9 \times 10^5$ to 0.327 at $Ra \simeq 4 \times 10^{10}$.

1. Introduction

Convection is ubiquitous in nature and in our everyday life. It can be found in the stars and planets, in the Earth's mantle and outer core, in the oceans and atmosphere, as well as in heat transport and mass mixing in many engineering applications. The paradigmatic example for natural convection is the Rayleigh-Bénard (RB) convection of an enclosed fluid layer between the colder top and the warmer bottom plates (Ahlers, Grossmann & Lohse 2009*b*; Lohse & Xia 2010). A key issue in the study of turbulent RB convection is to understand how heat is transported upwards across the fluid layer by convective flows. The global heat transport by convection is usually expressed in terms of the Nusselt number, namely,

$$Nu = \frac{QH}{\lambda_f \Delta}, \quad (1.1)$$

where Q is the heat current density across a fluid layer of thermal conductivity λ_f with height H and with an applied temperature difference Δ . The dynamics of the system is determined by the geometrical configuration of the convection cell and by two

[†] Email address for correspondence: qzhou@shu.edu.cn

dimensionless control parameters, i.e. the Rayleigh number and the Prandtl number,

$$Ra = \frac{\alpha g \Delta H^3}{\nu \kappa} \quad \text{and} \quad Pr = \frac{\nu}{\kappa}. \quad (1.2)$$

Here, g is the acceleration due to gravity and α , ν , and κ are the isobaric thermal expansion coefficient, the kinematic viscosity, and the thermal diffusivity of the working fluid, respectively. The cell geometry is usually described in terms of one or more aspect ratios, such as $\Gamma \equiv D/H$ for a cylindrical cell of inner diameter D and ($\Gamma_x \equiv L/H, \Gamma_y \equiv W/H$) for a rectangular cell of horizontal length L and width W . The Ra - and Pr -dependence of Nu for various working fluids and cell geometries have been studied, both experimentally and numerically, in great detail for many years (Castaing *et al.* 1989; Kerr 1996; Chavanne *et al.* 1997, 2001; Du & Tong 2000; Kerr & Herring 2000; Niemela *et al.* 2000; Ahlers & Xu 2001; Roche *et al.* 2002, 2005; Xia, Lam & Zhou 2002; Verzicco & Camussi 2003; Niemela & Sreenivasan 2003; Shishkina & Wagner 2007; Ahlers, Funfschilling & Bodenschatz 2009*a*; Funfschilling, Bodenschatz & Ahlers 2009; Song & Tong 2010; Stevens, Verzicco & Lohse 2010; Stevens, Lohse & Verzicco 2011*a*; Silano, Sreenivasan & Verzicco 2010; He *et al.* 2012). In addition, various theoretical models have been advanced to predict the behavior of convective heat transport (Castaing *et al.* 1989; Shraiman & Siggia 1990; Grossmann & Lohse 2000, 2001, 2003, 2004, 2011; Dubrulle 2001, 2002). For more detailed elucidation of the problem, we refer interested readers to the recent review paper by Ahlers *et al.* (2009*b*). On the other hand, there are fewer measurements focusing on the aspect-ratio-dependence (Xu, Bajaj & Ahlers 2000; Fleischer & Goldstein 2002; Cheung 2004; Nikolaenko *et al.* 2005; Funfschilling *et al.* 2005; Sun *et al.* 2005*a*; Niemela & Sreenivasan 2006; Roche *et al.* 2010), and those measurements were all performed in containers with a cylindrical geometry. The objective of the present experimental investigation is to fill this gap by making high-precision measurements of Nu over a wide range of the aspect ratio in convection cells with a rectangular geometry.

A lateral sidewall is indispensable for any convection experiment in the laboratory. The interaction between the sidewall and fluids would change the velocity and temperature distributions in the cell, and in turn change the flow structures of the system. Indeed, previous experimental studies for both cylindrical (du Puits, Resagk & Thess 2007) and rectangular (Xia, Sun & Cheung 2008) cells have shown that with increasing the aspect ratio the large-scale circulation (LSC) departs from a single-roll structure and becomes a multi-roll pattern. Thus, the Γ -dependence of Nu may reflect the influence of flow structures on heat transport characteristics via the influence on the boundary layers. Measurements in cylindrical samples using water as working fluid ($Pr \approx 4.3$) revealed that for $\Gamma \lesssim 6$ Nu decreases, albeit only a few percent, with increasing Γ (Funfschilling *et al.* 2005; Sun *et al.* 2005*a*). This suggests that the global heat transport properties of the RB system are not very sensitive to the flow structures for such parameter ranges. However, the situation is very different for lower Pr and for the two-dimensional (2D) case. Using 3D direct numerical simulation (DNS), Bailon-Cuba, Emran & Schumacher (2010) found for $Pr = 0.7$ that the minimum of Nu occurs at the aspect ratio where the LSC undergoes a transition from a single-roll to a double-roll structure and the variations in Nu for different Γ are significant and can yield 11.3% for $Ra = 10^8$. For 2D steady-state calculations, Ching & Tam (2006) obtained a power-law of $Nu \sim \Gamma^{-1}$ for $\Gamma \leq 3$. In 2D numerical RB flow, van der Poel, Stevens & Lohse (2011) identified different turbulent states for both $Pr = 0.7$ and 4.3, corresponding to different roll structures and associated with different overall heat transfers. Transitions among these states thus lead to jumps and sharp transitions in $Nu(\Gamma)$. By connecting the structures of $Nu(\Gamma)$ to the way the flow organizes itself in the sample, van der Poel *et al.* (2011) explained why the aspect-

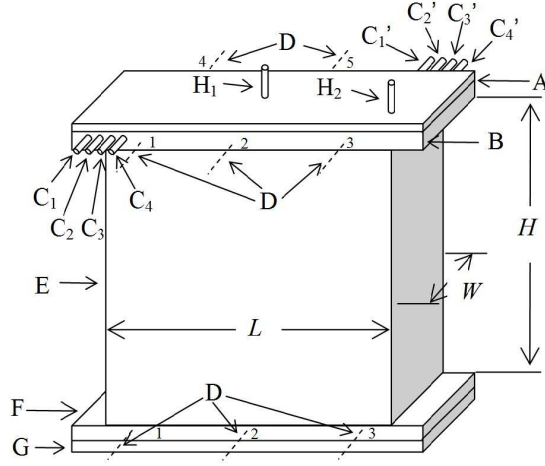


FIGURE 1. Schematic diagram of front view of a rectangular cell. A: the Plexiglas cover; B: the copper top plate; C_i and C_i' ($i = 1, 2, 3, 4$): nozzles connecting the channels to the refrigerated circulators; D: thermistors; E: the Plexiglas sidewall; F: the copper bottom plate; G: the copper cover for the bottom plate, H_1 : nozzle for transferring fluid into the cell; H_2 : nozzle for letting air out of the cell.

ratio dependence of Nu is more pronounced for small Pr . Compared with the 3D cases, we note that the 2D simulations show larger variations in $Nu(\Gamma)$ for both $Pr = 0.7$ and 4.3, which may be explained by the different flow structures formed in the 2D and 3D cases.

Different geometrical shapes represent different symmetries, and hence may lead to different features of the flow and heat transfer. This prompts us to study the Γ -dependence of Nu in a non-cylindrical system. In the present study, we choose rectangle as the shape of the cells, which has been widely used in the past (Xia, Sun & Zhou 2003; Gasteuil *et al.* 2007; Maystrenko, Resagk & Thess 2007; Zhou & Xia 2008, 2010*a,b*; Zhou *et al.* 2007, 2010). It was found that the convective flows in cells with such geometry share some similar dynamics as those in 2D RB system, such as the reversals of the LSC (Sugiyama *et al.* 2010).

The remainder of this paper is organized as follows. We give detailed descriptions of the experimental apparatus and conditions in §2. Experimental results are presented and analyzed in §3, which is divided into two parts. In §3.1, we compare the measured Nu for different aspect ratios and with those obtained in cylindrical cells. In §3.2 we consider the finite conductivity corrections of the top and bottom plates and estimate Nu_∞ for perfectly conducting plates. The scaling behaviors of Nu_∞ are also discussed in §3.2. We summarize our findings and conclude in §4.

2. Experimental apparatus and methods

Figure 1 is a schematic drawing of the front view of our apparatus and the drawing corresponds to $(\Gamma_x, \Gamma_y) = (1, 0.3)$. The sidewall of the cell, indicated as E in the figure, is composed by four transparent Plexiglas plates of 1.2 cm in thickness. The inner length L and inner width W of the cell are 50 cm and 15 cm, respectively. Six sidewalls of heights $H = 49.9, 25.0, 12.5, 6.9, 3.5,$ and 2.4 cm were used in the experiment. The corresponding aspect ratios are $(\Gamma_x \equiv L/H, \Gamma_y \equiv W/H) = (1, 0.3), (2, 0.6), (4, 1.2), (7.3, 2.2), (14.3, 4.3),$ and $(20.8, 6.3)$, respectively. As Γ_y is proportional to Γ_x , in the

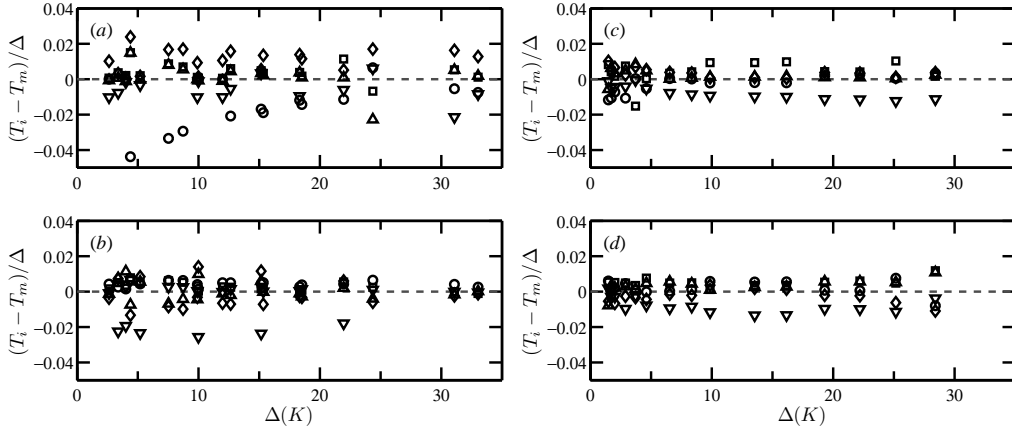


FIGURE 2. The normalized horizontal temperature differences, $(T_i - T_m)/\Delta$, for the top (a, c) and bottom (b, d) plates and for $\Gamma_x = 1$ (a, b) and 7.3 (c, d). The index i ($= 1, 2, 3, 4, 5$) of the thermistor is listed in figure 1 (see the top plate B and the bottom plate F).

remainder of the paper we use only Γ_x to indicate the cell's aspect ratio for ease of presentation. The top (B) and bottom (F) plates are made of pure copper of 56 cm in length and 21 cm in width and their fluid-contact surfaces are electroplated with a thin layer of nickel to prevent the oxidation by water. The thickness of the top plate is 3.5 cm and that of the bottom plate is 1.5 cm. Silicon O-rings are placed between the copper plates and the sidewall plates to avoid fluid leakage. Eight stainless steel posts (not shown) hold the top and bottom plates together. They are insulated from the plates by Teflon sleeves and washers. Four parallel channels (not shown) of 1.5 cm in width and 2 cm in depth are machined into the top plate and the separation between adjacent channels is 1.5 cm. The channels start and end, respectively, at the two diagonal ends of the long edges. A silicon rubber sheet (not shown) and a Plexiglas plate (A) of 1.4 cm in thickness are fixed on the top to form the cover and also to prevent interflow between the adjacent channels. At two ends of the i^{th} channel ($i = 1, 2, 3, 4$), there are two nozzles (C_i and C_i') located, through which the channel is connected to a separate refrigerated circulator (Polyscience 9712) that has a temperature stability of 0.01 °C. The channels and the circulators are connected such that the incoming cooler fluid and the outgoing warmer fluid in adjacent channels always flow in opposite directions. To provide constant and uniform heating, two rectangular Kapton film heaters of 25 cm in length and 15 cm in width are sandwiched between two copper plates (F and G) and are connected in parallel to a d.c. power supply (SGI 330X15D) with 99.99% long-term stability. Therefore, the experiments were conducted under constant heating of the bottom plate while maintaining a constant temperature at the top plate. Note that recent high-resolution 2D (Johnston & Doering 2009) and 3D (Stevens *et al.* 2011a) simulations have revealed that turbulent thermal convection with boundary conditions of constant temperature and constant heat flux display identical heat transport at sufficient high Rayleigh numbers.

Degassed water was used as the convecting fluid and the cell was leveled to better than 0.1°. During the measurements the entire cell was wrapped with several layers of Styrofoam. The temperature of each conducting plate was measured by five thermistors (D), which are embedded uniformly beneath the fluid-contact surface of the respective plate. When calculating the temperature difference Δ between the bottom and top plates, a correction was made for the temperature change between the thermistor position and

the fluid-contact surface. In each measurement after Ra was changed it took about 4 to 8 hours for the system to reach the steady state and we waited for at least 12 hours to start the measurements. A typical measurement lasted over 12 hours and more than 24 hours for low- Δ experiments ($\Delta < 4$ °C). No long-term drift of the mean temperature in the plates was observed over the duration of the measurement and the standard deviations were less than 0.5% of Δ for all measurements.

To see the temperature uniformity of each conducting plate, we plot in figure 2 the normalized temperature variation, $(T_i - T_m)/\Delta$, for both the top and bottom plates. Here, T_i ($i = 1, 2, 3, 4, 5$) is the time-averaged temperature measured by the i^{th} thermistor in a given plate and T_m is the mean value of all the five thermistors in the same plate. It is found that the $\Gamma_x = 1$ cell has the largest variation of plate temperature and we plot the $\Gamma_x = 1$ results in figures 2(a) and (b). The temperature variation for the other five Γ_x are similar and we choose $\Gamma_x = 7.3$ as an example and plot the results in figures 2(c) and (d). One sees that $(T_i - T_m)/\Delta$ is at most 4% for $\Gamma_x = 1$ and is less than 2% for all $\Gamma_x = 7.3$ measurements. We thus estimate that a systematic error of the order of 1% could be introduced into the measured Nu by this horizontal temperature inhomogeneity of the conducting plates. Several thermistors were placed around the cell sidewall and around the bottom plate to monitor the environment temperature, based on which heat leakages to the environment and conduction by the posts and Plexiglas sidewall were calculated. The relative leakages to the total heat current were found to become more significant with decreasing Δ and thus we kept heat leakages from all sources to be less than 7% of the total applied heat current by working with sufficiently large Δ . We found that the largest source of leakage, especially for the small aspect-ratio cells, is through the cell sidewall which is insulated by multi-layers of Styrofoam. The errors in calculating the leaks come mainly from uncertainties in the thermal conductivities of the material involved, which are estimated to be less than 20%. This translates into an uncertainty of less than 1.5% in the results of Nu .

3. Results and discussion

3.1. Nu vs. Ra for different Γ_x

The measured Nu with corresponding values of Δ , Ra , and Pr are given in tables 1 and 2. The $\Gamma_x = 1$ measurements were made at mean temperatures of 20°C and 30°C, corresponding to $Pr = 7.01$ and 5.45, respectively, and the measurements for the other five values of Γ_x were conducted at 31.3°C, corresponding to $Pr = 5.25$. Previous studies have revealed that with increasing Prandtl number Nu first increases, reaches its maximum value at around $Pr \approx 4$ (depends on Ra), and then decreases slightly or remains independent of Pr (Ahlers & Xu 2001; Grossmann & Lohse 2001; Xia *et al.* 2002; Silano *et al.* 2010; Stevens *et al.* 2011a). Therefore, within the present Pr range, Nu is expected to depend very weakly on Pr . Indeed, as shown in figures 3 and 5, no significant differences are observed between the $Pr = 5.45$ (circles) and 7.01 (right-triangles) results. Another source of uncertainty in the measured Nu could be the non-Boussinesq effects, as some of our measurements were made at larger Δ . Funfschilling *et al.* (2005) argued that the applied temperature difference Δ should be limited to $\lesssim 15$ °C to strictly conform to the Boussinesq conditions. However, it can be seen from figure 2 and tables 1 and 2 that some of our data have Δ much larger than 15°C. As we shall see below, the measured large- Δ data show the same trend as those of small Δ . This suggests that some of our data being not strictly Boussinesq will not change the main conclusions of the present work. Indeed, Ahlers *et al.* (2006) have shown that for water as the working

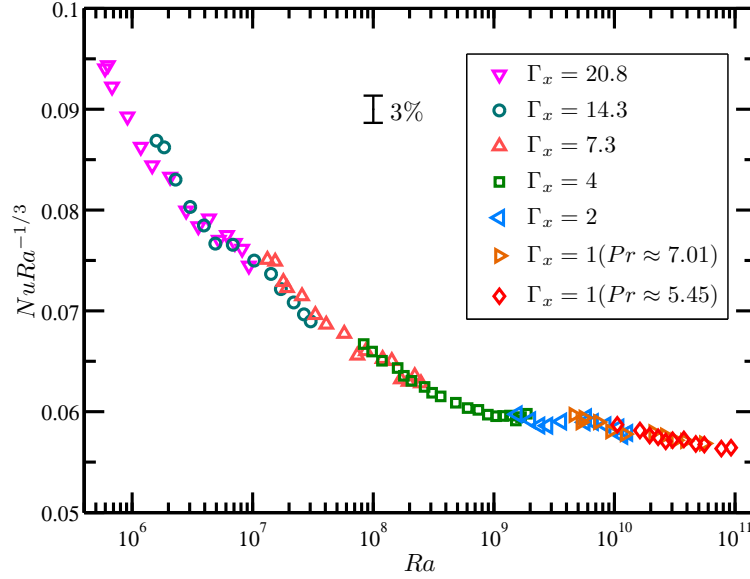


FIGURE 3. (color online). Compensated $Nu/Ra^{1/3}$ on a linear scale vs. Ra on a logarithmic scale. ∇ , $\Gamma_x = 20.8$; \circ , $\Gamma_x = 14.3$; \triangle , $\Gamma_x = 7.3$; \square , $\Gamma_x = 4$; \triangleleft , $\Gamma_x = 2$; \triangleright , $\Gamma_x = 1$ and $Pr \approx 7.01$; \diamond , $\Gamma_x = 1$ and $Pr \approx 5.45$. Note that the data are as measured, without the correction for the finite plate conductivity.

TABLE 1. Experimental parameters and results for the $\Gamma_x = 1$ cell. Here, Nu_∞ is calculated using Eq. (3.1) and the parameters $a = 0.275$ and $b = 0.39$ obtained by Brown *et al.* (2005) in cylindrical cells of two sets of plates of different thermal conductivities (Cu and Al). It is also seen that $\alpha\Delta \lesssim 0.01$ for all cases, which is considered to be sufficiently small. Note that two points are listed per line and the data are listed in chronological order.

Δ (K)	Ra	Pr	Nu	Nu_∞	$\alpha\Delta$ (10^{-3})	Δ (K)	Ra	Pr	Nu	Nu_∞	$\alpha\Delta$ (10^{-3})
$\Gamma_x = 1$											
3.44	1.06×10^{10}	5.45	128.8	130.3	1.04	5.24	1.63×10^{10}	5.41	147.4	149.5	1.59
15.16	4.73×10^{10}	5.40	205.5	210.6	4.62	18.33	5.57×10^{10}	5.48	216.6	222.4	5.49
24.36	7.71×10^{10}	5.40	239.8	247.2	7.42	9.97	3.03×10^{10}	5.47	178.3	181.9	2.99
12.65	3.77×10^{10}	5.52	191.9	196.2	3.74	7.52	2.30×10^{10}	5.46	163.5	166.4	2.27
6.41	1.96×10^{10}	5.46	155.4	157.9	1.93	8.74	2.66×10^{10}	5.47	170.4	173.6	2.63
30.93	9.27×10^{10}	5.51	255.3	264.0	9.19	5.30	9.25×10^9	7.01	121.9	123.1	1.09
7.02	1.22×10^{10}	7.02	133.1	134.6	1.44	3.20	5.56×10^9	7.02	105.3	106.1	0.66
11.98	2.11×10^{10}	6.98	160.2	162.8	2.49	4.23	7.34×10^9	7.03	114.6	115.6	0.87
15.10	2.64×10^{10}	7.01	171.6	174.7	3.12	2.63	4.60×10^9	7.00	99.3	100.0	0.54
21.96	3.87×10^{10}	6.99	193.1	197.3	4.56	3.02	5.26×10^9	7.02	102.5	103.2	0.62
31.40	5.55×10^{10}	6.98	216.9	222.5	6.54	18.52	3.23×10^{10}	7.02	182.0	185.6	3.82

fluid the non-Boussinesq effects could only slightly reduce the measured Nu by at most 1.4% for $\Delta = 40$ K and thus Nu is rather insensitive against even significant deviations from the Boussinesq conditions. Hence, for completeness all data are listed in the tables and are plotted in the figures.

Figure 3 shows $Nu/Ra^{1/3}$ as a function of Ra for all six Γ_x . It is seen that data points for $\Gamma_x = 20.8$ (down-triangles) collapse well on top of those for $\Gamma_x = 14.3$ (diamonds)

TABLE 2. Experimental results for the $\Gamma_x = 2, 4, 7.3, 14.3,$ and 20.8 cells. Note that two points are listed per line and the data are listed in chronological order.

Δ (K)	Ra	Pr	Nu	Nu_∞	$\alpha\Delta$ (10^{-3})	Δ (K)	Ra	Pr	Nu	Nu_∞	$\alpha\Delta$ (10^{-3})
$\Gamma_x = 2$											
17.18	6.67×10^9	5.26	111.0	114.1	5.41	9.39	3.64×10^9	5.26	90.8	92.6	2.95
21.63	8.46×10^9	5.24	119.5	123.2	6.84	7.12	2.79×10^9	5.23	82.5	84.0	2.25
33.33	1.28×10^{10}	5.28	135.6	140.5	11.0	6.02	2.40×10^9	5.19	78.5	79.7	1.92
29.86	1.17×10^{10}	5.23	130.7	135.3	9.45	14.62	5.69×10^9	5.25	105.3	107.9	4.61
5.17	2.01×10^9	5.25	74.7	75.8	1.63	27.15	1.08×10^{10}	5.18	129.3	133.8	8.37
14.94	5.85×10^9	5.25	106.1	108.9	4.57	3.82	1.56×10^9	5.23	69.2	70.1	1.21
$\Gamma_x = 4$											
17.02	8.90×10^8	5.25	57.4	59.1	5.36	1.60	8.33×10^7	5.25	29.1	29.4	0.50
35.83	1.88×10^9	5.25	73.8	76.8	11.3	2.26	1.18×10^8	5.25	31.9	32.3	0.71
32.61	1.68×10^9	5.29	70.7	73.4	10.2	3.03	1.59×10^8	5.24	34.9	35.3	0.96
29.21	1.52×10^9	5.26	68.0	70.5	9.18	5.10	2.67×10^8	5.26	40.2	40.9	1.61
25.98	1.36×10^9	5.25	66.0	68.4	8.19	6.93	3.62×10^8	5.25	43.9	44.7	2.18
22.96	1.19×10^9	5.27	63.2	65.3	7.20	9.16	4.83×10^8	5.23	47.8	48.8	2.90
19.87	1.04×10^9	5.24	60.4	62.3	6.28	11.66	6.06×10^8	5.27	51.1	52.3	3.66
14.25	7.44×10^8	5.26	54.5	56.0	4.49	3.96	2.07×10^8	5.25	37.3	37.9	1.25
1.87	9.78×10^7	5.26	30.4	30.7	0.59	5.88	3.08×10^8	5.25	41.8	42.5	1.85
3.44	1.79×10^8	5.26	35.9	36.4	1.08						
$\Gamma_x = 7.3$											
16.16	1.42×10^8	5.24	34.0	35.1	5.10	2.91	2.57×10^7	5.25	21.1	21.4	0.92
13.53	1.20×10^8	5.24	32.1	33.1	4.27	4.63	4.08×10^7	5.25	23.6	24.1	1.46
22.21	1.96×10^8	5.25	36.6	37.9	7.01	2.18	1.92×10^7	5.25	19.4	19.6	0.69
9.87	8.69×10^7	5.25	29.2	30.0	3.11	1.75	1.54×10^7	5.25	18.6	18.9	0.55
6.55	5.74×10^7	5.26	26.1	26.7	2.06	3.74	3.31×10^7	5.24	22.3	22.7	1.18
1.51	1.32×10^7	5.26	17.8	18.0	0.47	25.14	2.21×10^8	5.26	38.4	39.9	7.91
8.36	7.37×10^7	5.25	27.5	28.2	2.64	28.43	2.49×10^8	5.27	39.5	41.1	8.93
2.04	1.80×10^7	5.25	19.1	19.3	0.64	19.31	1.69×10^8	5.26	35.0	36.1	6.07
$\Gamma_x = 14.3$											
12.35	1.42×10^7	5.25	17.8	18.4	3.89	2.65	3.03×10^6	5.26	11.6	11.8	0.83
8.96	1.03×10^7	5.26	16.3	16.8	2.82	1.61	1.84×10^6	5.26	10.6	10.7	0.51
5.98	6.84×10^6	5.27	14.5	14.9	1.88	14.95	1.71×10^7	5.26	18.6	19.3	4.70
2.00	2.29×10^6	5.26	10.9	11.1	0.63	18.96	2.19×10^7	5.24	19.8	20.6	5.99
3.44	3.94×10^6	5.26	12.4	12.6	1.08	23.45	2.66×10^7	5.28	20.8	21.7	7.34
4.28	4.90×10^6	5.26	13.0	13.3	1.35	26.52	3.02×10^7	5.27	21.5	22.4	8.32
1.39	1.59×10^6	5.26	10.1	10.3	0.44						
$\Gamma_x = 20.8$											
11.75	4.34×10^6	5.26	12.9	13.4	3.70	3.19	1.18×10^6	5.26	9.1	9.3	1.01
16.55	6.12×10^6	5.26	14.2	14.8	5.21	5.59	2.07×10^6	5.26	10.6	10.9	1.76
19.15	7.11×10^6	5.24	14.8	15.4	6.05	1.85	6.82×10^5	5.27	8.1	8.3	0.58
22.00	8.18×10^6	5.24	15.3	16.0	6.95	3.97	1.47×10^6	5.26	9.6	9.8	1.25
14.18	5.24×10^6	5.26	13.4	13.9	4.46	2.48	9.16×10^5	5.26	8.7	8.8	0.78
7.51	2.81×10^6	5.23	11.3	11.6	2.38	1.71	6.30×10^5	5.26	8.1	8.2	0.54
9.59	3.55×10^6	5.25	12.0	12.3	3.02	25.00	9.30×10^6	5.24	15.7	16.4	7.90
1.62	5.96×10^5	5.26	7.9	8.1	0.51						

(within their overlap Ra -range), which in turn collapse well on top of those for $\Gamma_x = 7.3$ (up-triangles). This implies that all sets of data can be described by a single curve over such a wide range of Γ_x , i.e., no significant Γ_x -dependence is observed. As discussed in §1, Γ -dependence of Nu essentially reflects the influence of flow structures on heat transport

characteristics. Indeed, using particle image velocimetry (PIV), Xia *et al.* (2008) have shown in rectangular cells that the number of the convection rolls depends systematically on the aspect ratio of the system: only one convection roll is observed in the $\Gamma_x = 1$ and 2 cells and the LSC breaks into (horizontally arranging) multi-roll structure for Γ_x larger than or equal to 4. Therefore, our present results suggest that for rectangular geometry turbulent heat transport is very insensitive to the nature and structures of the large-scale mean flows of the system. We note that our present results are different from those obtained in 2D numerical case (van der Poel *et al.* 2011), which were made for both $Pr = 0.7$ and 4.3. For the 2D simulation, the stable states with n rolls are found to enable larger heat transfer than those with $n + 1$ rolls for vertically arranging LSC rolls. One possible reason for this difference may be attributed to different alignments of the LSC rolls, i.e. the aspect ratios of the 2D simulation vary between 0.4 and 1.25 and the LSC rolls are stacked vertically, whereas for the present geometry we have horizontally stacked rolls (Xia *et al.* 2008).

In figure 4, we compare the present results with those obtained in cylindrical cells and at $Pr \approx 4.4$. We mainly consider two recent data sets: one is from Funfschilling *et al.* (2005) (referred to as FBNA) and the other is from Sun *et al.* (2005a) (referred to as SRSX). As our measured Nu is independent of the cells' aspect ratio, here we do not distinguish our data for different Γ_x . Note that all data in figure 4 are as measured, without the correction for the finite plate conductivity. For the FBNA data, one sees that the $\Gamma = 6$ data of FBNA are in excellent agreement with ours, but their small- Γ data are a few percent larger. Nevertheless, we note that the $\Gamma = 1$ data of FBNA (down-triangles) show similar trends to ours for $Ra \lesssim 10^9$ and $Ra \gtrsim 10^{10}$ and thus the small difference between the two sets of data may be attributed to different system errors. The SRSX data and ours are much closer. One sees that parts of the $\Gamma = 5$ and 10 data of SRSX agree well with ours and the others lie slightly below our measured Nu .

One noticeable difference between the present results and those of FBNA and SRSX is worthy of note. For both FBNA and SRSX the larger- Γ results lie consistently below those of smaller ones, i.e. Nu is generally smaller for larger Γ . This is true even for the largest- Γ (i.e. $\Gamma = 10$ and 20) data of SRSX (see figure 4). Whereas, our measured Nu for all six values of Γ_x fall into a single curve, i.e. Nu is essentially independent of Γ_x for our results. To understand such a difference, we note that all data plotted in figure 4 have not been corrected for the influence of the finite conductivity of the top and bottom plates (Verzicco 2004). In a cylindrical cell of $\Gamma = 0.5$, Sun, Xi & Xia (2005b) argued that because of the finite conductivity and finite heat capacity of the plates the azimuthal sweeping of the circulation plane of the LSC would make heat transfer more efficient than the case when the LSC is locked in a particular orientation. Moreover, Xi & Xia (2008) studied the azimuthal motion of the LSC in cylindrical cells of $\Gamma = 0.5, 1.0$, and 2.3 and their results showed that the LSC's azimuthal motion is more confined in larger- Γ cells. If we generalize the above two findings to large Γ and taken them together, a possible scenario can be achieved: the larger- Γ cell confines the azimuthal sweeping motion of the LSC which in turn reduces the measured Nu . This scenario could be valid for cylindrical cells due to their azimuthal symmetry. But for rectangular cells, this is not expected to work because the rectangular geometry has already locked the orientation of the LSC (Xia *et al.* 2003). Therefore, our present Γ_x -independent results are consistent with the lack of the azimuthal sweeping motion of the LSC in rectangular cells. What we should stress is that the large- Γ cell contains multi-roll structures of the LSC (du Puits *et al.* 2007; Xia *et al.* 2008; Bailon-cuba *et al.* 2010) and thus the azimuthal motion of the LSC and its influence on heat transfer should be more complicated for large Γ . However, as we shall see in figure 6, when corrections for the finite conductivity of the plates are

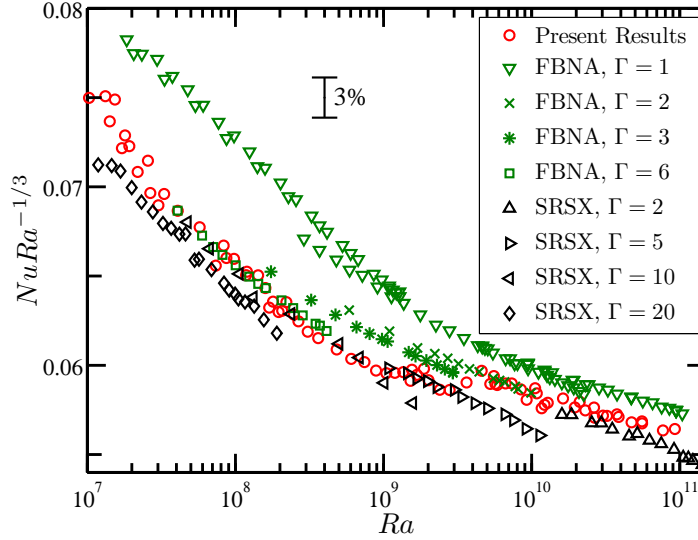


FIGURE 4. (color online). Comparison among $Nu/Ra^{-1/3}$ from the present work (\circ), from Funfschilling *et al.* (2005) (∇ , $\Gamma = 1$; \times , $\Gamma = 2$; $*$, $\Gamma = 3$; \square , $\Gamma = 6$; for clarity their $\Gamma = 1.5$ data are not shown) and from Sun *et al.* (2005a) (\triangle , $\Gamma = 2$; \triangleright , $\Gamma = 5$; \triangleleft , $\Gamma = 10$; \diamond , $\Gamma = 20$). As our results show that for rectangular geometry $Nu/Ra^{-1/3}$ is independent of the cells' aspect ratio, here we do not distinguish our data for different Γ_x . Note that all data are as measured, without the correction for the finite plate conductivity.

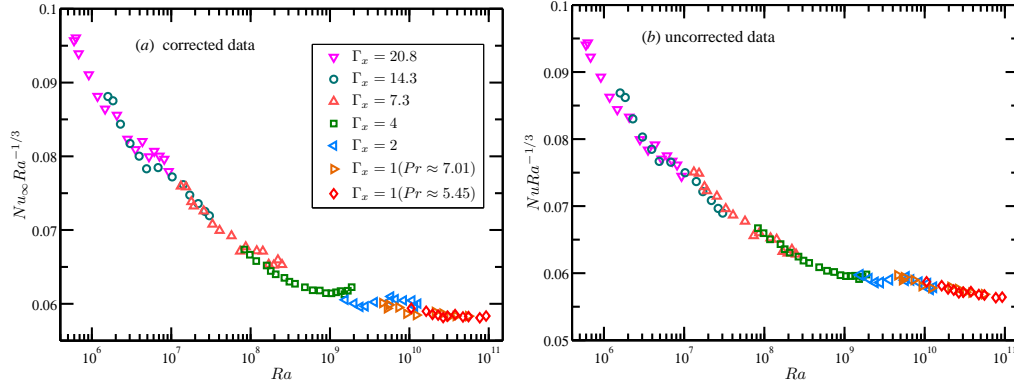


FIGURE 5. (color online). (a) Compensated $Nu_{\infty}/Ra^{1/3}$ on a linear scale vs. Ra on a logarithmic scale: symbols as figure 3. Here, Nu_{∞} is calculated using Eq. (3.1) and the parameters $a = 0.275$ and $b = 0.39$ obtained by Brown *et al.* (2005) in cylindrical cells. For comparison, the uncorrected data $Nu/Ra^{1/3}$ of figure 3 are replotted in (b).

made, Γ -dependence of Nu_{∞} becomes weaker for both the FBNA and SRSX data, which suggests that the finite plate conductivity effect is indeed a major factor for the observed difference of the behaviors of heat transfer in rectangular and cylindrical cells.

3.2. Nu_{∞} vs. Ra for different Γ_x

Brown *et al.* (2005) suggested an empirical correction factor $f(X) = 1 - \exp[-(aX)^b]$, namely

$$Nu = f(X)Nu_{\infty} = \{1 - \exp[-(aX)^b]\}Nu_{\infty}(Ra, Pr), \quad (3.1)$$

to obtain estimates of the ideal Nusselt number Nu_∞ for plates with perfect conductivity from the measured Nu . Here, $X = R_f/R_p$ is the ratio of the effective thermal resistance of the working fluid, $R_f = H/(\lambda_f Nu)$, to the thermal resistance of the plates, $R_p = e/\lambda_p$, λ_p ($= 401$ W/m K) is the conductivity of plates (Cu), λ_f ($\lambda_f = 0.614$ W/m K for $Pr = 5.25$ and $\lambda_f = 0.589$ W/m K for $Pr = 7$) is the conductivity of water, and e ($= 1.5$ cm) is the mean thickness of the top (the part of the top plate below the cooling channels is used here) and bottom plates (Verzicco 2004). To apply the relation (3.1) to our measured Nu , one needs to determine the values of a and b . The best way to do this is to use plates of different thermal conductivities, as was done by Brown *et al.* (2005), who used two sets of plates made of Cu and Al. However, the lack of aluminum-plate measurements in the present study prevents us to determine the values of a and b . Alternatively, to estimate Nu_∞ , we use the parameters $a = 0.275$ and $b = 0.39$ obtained by Brown *et al.* (2005) in cylindrical samples of 50 cm in diameter.

Figure 5(a) shows the calculated $Nu_\infty/Ra^{1/3}$ as a function of Ra . For comparison, the uncorrected data $Nu/Ra^{1/3}$ of figure 3 are replotted in figure 5(b). The corrected data in figure 5(a) seem to display a small aspect ratio dependence, e.g., near $Ra = 2 \times 10^8$ the $\Gamma_x = 7.3$ data lie slightly above the $\Gamma_x = 4$ data and near $Ra = 2 \times 10^9$ the $\Gamma_x = 4$ data lie slightly above the $\Gamma_x = 2$ data. We note that this dependence is consistent with the FBNA data (see figure 6, where data points for $\Gamma = 6$ lie slightly above those for $\Gamma = 3$, which in turn lie slightly above those for $\Gamma = 2$). Nevertheless, the differences of Nu_∞ for the two adjacent- Γ_x sets of data are only a few percent, which is smaller than or comparable with the experimental errors. Hence, we may also conclude that no significant Γ_x -dependence of heat transfer is observed.

We want to emphasize that here we adopted the parameters of $a = 0.275$ and $b = 0.39$ determined by Brown *et al.* (2005) for cylindrical samples with a diameter of 50 cm. Brown *et al.* (2005) have shown experimentally that a and b are independent of the aspect ratio, but vary with the diameter of the sample. In the present study, we chose the rectangle as the geometry of the convection cells, which can possibly have an influence on the finite plate correction, as we have discussed at the end of § 3.1. However, without the measurement performed with aluminum plates it is difficult to assess whether the geometry would (significantly) influence the values of a and b . By using different sets of a and b to perform the finite conductivity correction, we estimate that the uncertainties of a and b may yield a few percent uncertainty on the obtained Nu_∞ , which is the same order of the difference between Nu and Nu_∞ . We should also stress that the best way to estimate Nu_∞ is to use plates with different thermal conductivities, as was done by Brown *et al.* (2005) for cylindrical samples. Therefore, new measurements with Al plates are essential for concretely settling the problem and this will be the objective of future studies.

In figure 6 we directly compare our Nu_∞ and those of FBNA and SRSX. It is seen that our data display the similar Ra -dependence as the $\Gamma = 1$ data of FBNA, and an excellent agreement between our data and those of SRSX can be found for nearly all the overlap Ra range. As the three sets of data were taken independently from the samples with very different geometries, this agreement is just remarkable.

Finally, we studied the power-law relation between Nu_∞ and Ra , namely,

$$Nu_\infty = A(\Gamma_x)Ra^{\beta(\Gamma_x)}. \quad (3.2)$$

Table 3 displays the fitted results for the power-law relation (3.2) at fixed aspect ratios. One sees that as Γ_x increases in general the prefactor A increases and the scaling exponent β decreases. Here, Γ_x -dependences of A and β essentially reflect their Ra -dependence as our results do not reveal significant aspect-ratio dependence of Nu_∞ . We thus do not

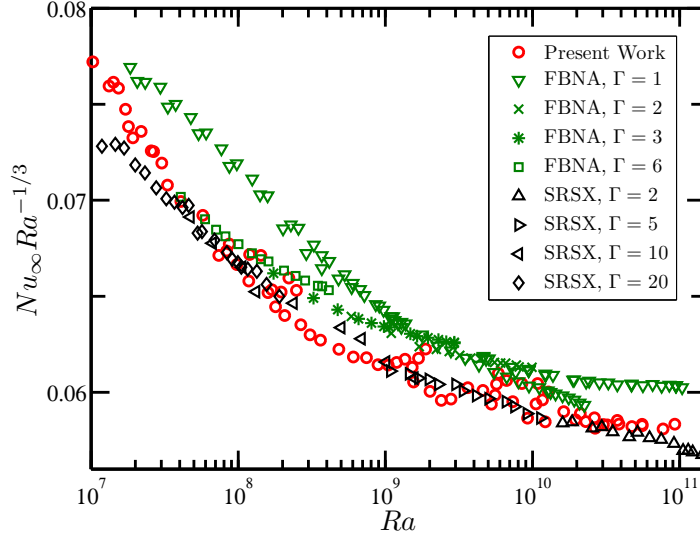


FIGURE 6. (color online). Comparison among $Nu_\infty/Ra^{-1/3}$ from the present work, from Funfschilling *et al.* (2005), and from Sun *et al.* (2005a). Note that the data have been corrected for the finite plate conductivity.

TABLE 3. Fitted parameters from equations (3.2).

Γ_x	1	2	4	7.3	14.3	20.8
$A(\Gamma_x)$	0.074	0.059	0.108	0.173	0.212	0.242
$\beta(\Gamma_x)$	0.324	0.335	0.307	0.282	0.271	0.262

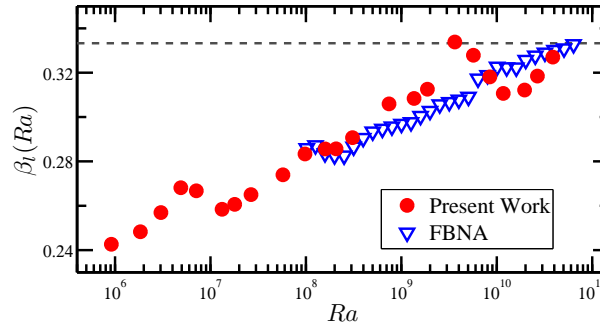


FIGURE 7. (color online). Local scaling exponent β_l of $Nu_\infty(Ra)$, determined from a power-law fit over a sliding window of half a decade, as a function of Ra for the present data (solid circles) and for the $\Gamma = 1$ data of Funfschilling *et al.* (2005) (open triangles). Dashed line marks $\beta_l = 1/3$ for reference. Note that both sets of β_l were obtained from the corrected data.

distinguish the data for different Γ_x and take them together to study the scaling behaviors of $Nu_\infty(Ra)$. The local scaling exponent β_l is obtained by a power-law fit, $Nu_\infty \sim Ra^{\beta_l}$, to the data for $Nu_\infty(Ra)$ within a sliding window that covers half a decade of Ra . Figure 7 shows the results for β_l as a function of Ra . It is seen that β_l roughly increases linearly with $\log Ra$ from $\beta_l = 0.243$ at $Ra \approx 9 \times 10^5$ to $\beta_l = 0.342$ at $Ra \approx 3.6 \times 10^9$. At small Ra , our results differ very much from the DNS results for cylindrical samples of unit

aspect ratio by Wagner, Shishkina & Wagner (2012), who found that β_l increases again as Ra decreases below 2×10^7 and grows to about 0.30 at $Ra = 10^6$ [see figure 2 of Wagner *et al.* (2012)]. The apparent differences in β_l may be explained by the different Prandtl number in the two studies, i.e., Wagner *et al.* (2012) carried out their simulations at $Pr = 0.786$, while our measurements were made at $Pr \approx 5.45$. For higher Ra , β_l drops slightly and fluctuates around 0.32. The FBNA results for β_l are also displayed together with ours in figure 7 for comparison. For $Ra \geq 10^8$ the two data sets both increase with Ra with ours being a little scatter. A source of uncertainty for our data could be the non-Boussinesq effect, i.e. the FBNA data were obtained in the strictly Boussinesq range, while some of our data are beyond the Boussinesq range (i.e. $\Delta > 15^\circ\text{C}$). However, as have discussed in §3.1, some of our data being not strictly Boussinesq will not change our main conclusions. What is worthy of note is that around $Ra \approx 10^{10}$ our measured β_l has a value that is close to the value of $1/3$. The exponent $\beta \approx 1/3$ was obtained before in cylindrical cells of $\Gamma = 1$ by FBNA at $Ra \approx 7 \times 10^{10}$ (see open triangles in figure 7) and of $\Gamma = 4$ by Niemela & Sreenivasan (2006) for $Ra > 10^{10}$. Here, our results in rectangular cells seem to be qualitatively consistent with these findings

4. Conclusion

In conclusion, our high-precision measurements of Nu in rectangular cells with (Γ_x, Γ_y) varying from (1, 0.3) to (20.8, 6.3) show that Nu is independent of the aspect ratio. This is slightly different from the observations by both FBNA and SRSX in cylindrical cells where Nu is found to be in general a decreasing function of Γ , at least for $\Gamma \sim 1$ and larger. Such a difference may be attributed to different azimuthal dynamics of the large-scale circulation (LSC) and is probably a manifestation of the finite plate conductivity effect. To make finite conductivity corrections, an empirical correction factor $f(X) = 1 - \exp[-(aX)^b]$, together with the parameters $a = 0.275$ and $b = 0.39$ obtained by Brown *et al.* (2005) in cylindrical samples, were adopted to estimate Nu_∞ for plates with perfect conductivity from the measured Nu . The obtained Nu_∞ were found to be consistent with the FBNA and SRSX data measured in cylindrical samples to only a few percent. The scaling behaviors between Nu_∞ and Ra were studied for all six aspect ratios. The local scaling exponents β_l of $Nu_\infty \sim Ra^{\beta_l}$ were calculated and found to increase with increasing Ra . Around $Ra \approx 10^{10}$ our measured β_l has a value that is close to the value of $1/3$.

This work was supported by the Natural Science Foundation of China (Nos. 11161160554, 11002085, and 11032007) and Shanghai Program for Innovative Research Team in Universities.

REFERENCES

- AHLERS, G., BROWN, B., ARAUJO, F. F., FUNFSCHILLING, D., GROSSMANN, S. & LOHSE, D. 2006a Non-Oberbeck-Boussinesq effects in strongly turbulent Rayleigh–Bénard convection. *J. Fluid Mech.* **569**, 409–445.
- AHLERS, G., FUNFSCHILLING, D. & BODENSCHATZ, E. 2009a Transitions in heat transport by turbulent convection at Rayleigh numbers up to 10^{15} . *New J. Phys.* **11**, 123001.
- AHLERS, G., GROSSMANN, S. & LOHSE, D. 2009b Heat transfer and large scale dynamics in turbulent Rayleigh–Bénard convection. *Rev. Mod. Phys.* **81**, 503–537.
- AHLERS, G. & XU, X.-C. 2001 Prandtl-number dependence of heat transport in turbulent Rayleigh–Bénard convection. *Phys. Rev. Lett.* **86**, 3320–3323.
- BAILON-CUBA, J., EMRAN, M. S. & SCHUMACHER, J. 2010 Aspect ratio dependence of heat transfer and large-scale flow in turbulent convection. *J. Fluid Mech.* **655**, 152–173.

- BROWN, E., NIKOLAENKO, A., FUNFSCHILLING, D. & AHLERS, G. 2005 Heat transport in turbulent Rayleigh-Bénard convection: effect of finite top- and bottom-plate conductivities. *Phys. Fluids* **17**, 075108.
- CASTAING, B., GUNARATNE, G., HESLOT, F., KADANOFF, L., LIBCHABER, A., THOMAE, S., WU, X.-Z., ZALESKI, S. & ZANETTI, G. 1989 Scaling of hard thermal turbulence in Rayleigh-Bénard convection. *J. Fluid Mech.* **204**, 1–30.
- CHAVANNE, X., CHILLA, F., CASTAING, B., HEBRAL, B., CHABAUD, B. & CHAUSSY, J. 1997 Observation of the Ultimate Regime in Rayleigh-Bénard convection. *Phys. Rev. Lett.* **79**, 3648–3651.
- CHAVANNE, X., CHILLA, F., CHABAUD, B., CASTAING, B. & HEBRAL, B. 2001 Turbulent Rayleigh-Bénard convection in gaseous and liquid He. *Phys. Fluids* **13**, 1300–1320.
- CHEUNG, Y. H. 2004 Aspect-ratio dependence of the Nusselt number and boundary layer properties in Rayleigh-Bénard turbulent convection. MPhil thesis, The Chinese University of Hong Kong.
- CHING, E. S. C. & TAM, W. S. 2006 Aspect-ratio dependence of heat transport by turbulent Rayleigh-Bénard convection. *J. Turb.* **7**, 72.
- DU, Y.-B. & TONG, P. 2000 Turbulent thermal convection in a cell with ordered rough boundaries. *J. Fluid Mech.* **407**, 57–84.
- DUBRULLE, B. 2001 Logarithmic corrections to scaling in turbulent thermal convection. *Eur. Phys. J. B* **21**, 295–304.
- DUBRULLE, B. 2002 Scaling in large Prandtl number turbulent thermal convection. *Eur. Phys. J. B* **28**, 361–367.
- FLEISCHER, A. S. & GOLDSTEIN, R. J. 2002 High-Rayleigh-number convection of pressurized gases in a horizontal enclosure. *J. Fluid Mech.* **469**, 1–12.
- FUNFSCHILLING, D., BODENSCHATZ, E. & AHLERS, G. 2009 Search for the "Ultimate State" in turbulent Rayleigh-Bénard convection. *Phys. Rev. Lett.* **103**, 014503.
- FUNFSCHILLING, D., BROWN, E., NIKOLAENKO, A. & AHLERS, G. 2005 Heat transport by turbulent Rayleigh-Bénard convection in cylindrical samples with aspect ratio one and larger. *J. Fluid Mech.* **536**, 145–154.
- GASTEUIL, Y., SHEW, W. L., GIBERT, M., CHILLA, F., CASTAING, B. & PINTON, J.-F. 2007 Lagrangian temperature, velocity, and local heat flux measurement in Rayleigh-Bénard convection. *Phys. Rev. Lett.* **99**, 234302.
- GROSSMANN, S. & LOHSE, D. 2000 Scaling in thermal convection: a unifying theory. *J. Fluid Mech.* **407**, 27–56.
- GROSSMANN, S. & LOHSE, D. 2001 Thermal convection for large Prandtl numbers. *Phys. Rev. Lett.* **86**, 3316–3319.
- GROSSMANN, S. & LOHSE, D. 2003 On geometry effects in Rayleigh-Bénard convection. *J. Fluid Mech.* **486**, 105–114.
- GROSSMANN, S. & LOHSE, D. 2004 Fluctuations in turbulent Rayleigh-Bénard convection: The role of plumes. *Phys. Fluids* **16**, 4462.
- GROSSMANN, S. & LOHSE, D. 2011 Multiple scaling in the ultimate regime of thermal convection. *Phys. Fluids* **23**, 045108.
- HE, X.-Z., FUNFSCHILLING, D., NOBACH, H., BODENSCHATZ, E. & AHLERS, G. 2012 Transition to the ultimate state of turbulent Rayleigh-Bénard convection. *Phys. Rev. Lett.* **108**, 024502.
- KERR, R. M. & HERRING, J. 2000 Prandtl number dependence of Nusselt number in direct numerical simulations. *J. Fluid Mech.* **491**, 325–344.
- JOHNSTON, H. & DOERING, C. R. 2009 Comparison of turbulent thermal convection between conditions of constant temperature and constant flux. *Phys. Rev. Lett.* **102**, 064501.
- LOHSE, D. & XIA, K.-Q. 2010 Small-scale properties of turbulent Rayleigh-Bénard convection. *Annu. Rev. Fluid Mech.* **42**, 335–64.
- MAYSTRENKO, A., RESAGK, C. & THESS, A. 2007 Structure of the thermal boundary layer for turbulent Rayleigh-Bénard convection of air in a long rectangular enclosure. *Phys. Rev. E* **75**, 066303.
- NIEMELA, J. J., SKRBEK, L., SREENIVASAN, K. R. & DONNELLY, R. J. 2000 Turbulent convection at very high Rayleigh numbers. *Nature* **404**, 837–840.

- NIEMELA, J. J. & SREENIVASAN, K. R. 2003 Confined turbulent convection. *J. Fluid Mech.* **481**, 355–384.
- NIEMELA, J. J. & SREENIVASAN, K. R. 2006 Turbulent convection at high Rayleigh numbers and aspect ratio 4. *J. Fluid Mech.* **557**, 411–422.
- NIKOLAENKO, A., BROWN, E., FUNFSCHILLING, D. & AHLERS, G. 2005 Heat transport by turbulent Rayleigh-Bénard convection in cylindrical cells with aspect ratio one and less. *J. Fluid Mech.* **523**, 251–260.
- VAN DER POEL, E. P., STEVENS, R. J. A. M. & LOHSE, D. 2011 Connecting flow structures and heat flux in turbulent Rayleigh-Bénard convection. *Phys. Rev. E* **84**, 045303(R).
- PRESS, W. H., TEUKOLSKY, S., VETTERLING, W. & FLANNERY, B. 1986 *Numerical Recipes*. Cambridge University Press, Cambridge, UK.
- DU PUIITS, R., RESAGK, C. & THESS, A. 2007 Breakdown of wind in turbulent thermal convection. *Phys. Rev. E* **75**, 016302.
- KERR, R. M. 1996 *J. Fluid Mech.* **310**, 139.
- ROCHE, P.-E., CASTAING, B., CHABAUD, B. & HÉBRAL, B. 2002 Prandtl and Rayleigh numbers dependences in Rayleigh-Bénard convection. *Europhys. Lett.* **58**, 693–698.
- ROCHE, P.-E., GAUTHIER, F., CHABAUD, B. & HÉBRAL, B. 2005 Ultimate regime of convection: Robustness to poor thermal reservoirs. *Phys. Fluids* **17**, 115107.
- ROCHE, P.-E., GAUTHIER, F., KAISER, R. & SALORT, J. 2010 On the triggering of the Ultimate Regime of convection. *New J. Phys.* **12**, 085014.
- SHISHKINA, O. & WAGNER, C. 2007 Local heat fluxes in turbulent Rayleigh-Bénard convection. *Phys. Fluids* **19**, 085107.
- SHRAIMAN, B. I. & SIGGIA, E. D. 1990 Heat transport in high-Rayleigh-number convection. *Phys. Rev. A* **42**, 3650–3653.
- SILANO, G., SREENIVASAN, K. R. & VERZICCO, R. 2010 Numerical simulations of Rayleigh-Bénard convection for Prandtl numbers between 10^{-1} and 10^4 and Rayleigh numbers between 10^5 and 10^9 . *J. Fluid Mech.* **662**, 409–446.
- SONG, H. & TONG, P. 2010 Scaling laws in turbulent Rayleigh-Bénard convection under different geometry. *Europhys. Lett.* **90**, 44001.
- STEVENS, R. J. A. M., LOHSE, D. & VERZICCO, R. 2011a Prandtl and Rayleigh number dependence of heat transport in high Rayleigh number thermal convection. *J. Fluid Mech.* **688**, 31–43.
- STEVENS, R. J. A. M., VERZICCO, R. & LOHSE, D. 2010 Radial boundary layer structure and Nusselt number in Rayleigh-Bénard convection. *J. Fluid Mech.* **643**, 495–507.
- SUGIYAMA, K., NI, R., STEVENS, R. J. A. M., CHAN, T.-S., ZHOU, S.-Q., XI, H.-D., SUN, C., GROSSMANN, S., XIA, K.-Q. & LOHSE, D. 2010 Flow reversals in thermally driven turbulence. *Phys. Rev. Lett.* **105**, 034503.
- SUN, C., REN, L.-Y., SONG, H. & XIA, K.-Q. 2005a Heat transport by turbulent Rayleigh-Bénard convection in 1 m diameter cylindrical cells of widely varying aspect ratio. *J. Fluid Mech.* **542**, 165–174.
- SUN, C., XI, H.-D. & XIA, K.-Q. 2005b Azimuthal symmetry, flow dynamics, and heat transport in turbulent thermal convection in a cylinder with an aspect ratio of 0.5. *Phys. Rev. Lett.* **95**, 074502.
- VERZICCO, R. 2004 Effects of nonperfect thermal sources in turbulent thermal convection. *Phys. Fluids* **16**, 1965–1979.
- VERZICCO, R. & CAMUSSI, R. 2003 Numerical experiments on strongly turbulent thermal convection in a slender cylindrical cell. *J. Fluid Mech.* **477**, 19–49.
- WAGNER, S., SHISHKINA, O. & WAGNER, C. 2012 Boundary layers and wind in cylindrical Rayleigh-Bénard cells. *J. Fluid Mech.* **697**, 336–366.
- WEISS, S., STEVENS, R. J. A. M., ZHONG, J.-Q., CLERCX, H. J. H., LOHSE, D. & AHLERS, G. 2010 Finite-size effects lead to supercritical bifurcations in turbulent rotating Rayleigh-Bénard convection. *Phys. Rev. Lett.* **105**, 224501.
- XI, H.-D. & XIA, K.-Q. 2008 Azimuthal motion, reorientation, cessation, and reversal of the large-scale circulation in turbulent thermal convection: a comparative study in aspect ratio one and one-half geometries. *Phys. Rev. E* **78**, 036326.
- XIA, K.-Q., LAM, S. & ZHOU, S.-Q. 2002 Heat-flux measurement in high-Prandtl-number turbulent Rayleigh-Bénard convection. *Phys. Rev. Lett.* **88**, 064501.

- XIA, K.-Q., SUN, C. & CHEUNG, Y.-H. 2008 Large scale velocity structures in turbulent thermal convection with widely varying aspect ratio. *14th Int Symp on Application of Laser Techniques to Fluid Mechanics* .
- XIA, K.-Q., SUN, C. & ZHOU, S.-Q. 2003 Particle image velocimetry measurement of the velocity field in turbulent thermal convection. *Phys. Rev. E* **68**, 066303.
- XU, X.-C., BAJAJ, K. M. S. & AHLERS, G. 2000 Heat transport in turbulent Rayleigh-Bénard convection. *Phys. Rev. Lett.* **84**, 4357–4360.
- ZHOU, Q., STEVENS, R. J. A. M., SUGIYAMA, K., GROSSMANN, S., LOHSE, D. & XIA, K.-Q. 2010 Prandtl-Blasius temperature and velocity boundary-layer profiles in turbulent Rayleigh-Bénard convection. *J. Fluid Mech.* **664**, 297–312.
- ZHOU, Q. & XIA, K.-Q. 2008 Comparative experimental study of local mixing of active and passive scalars in turbulent thermal convection. *Phys. Rev. E* **77**, 056312.
- ZHOU, Q. & XIA, K.-Q. 2010*a* Measured instantaneous viscous boundary layer in turbulent Rayleigh-Bénard convection. *Phys. Rev. Lett.* **104**, 104301.
- ZHOU, Q. & XIA, K.-Q. 2010*b* The mixing evolution and geometric properties of a passive scalar field in turbulent Rayleigh-Bénard convection. *New J. Phys.* **12**, 083029.
- ZHOU, S.-Q., SUN, C. & XIA, K.-Q. 2007 Measured oscillations of the velocity and temperature fields in turbulent Rayleigh-Bénard convection in a rectangular cell. *Phys. Rev. E* **76**, 036301.